ELSEVIER

Contents lists available at ScienceDirect

# Composites Part B

journal homepage: www.elsevier.com/locate/compositesb



# Strengthening sandwich composites by laminating ultra-thin oriented carbon nanotube sheets at the skin/core interface

Dongyang Cao <sup>a</sup>, Tingge Xu <sup>a</sup>, Mengmeng Zhang <sup>b</sup>, Zhong Wang <sup>b</sup>, D. Todd Griffith <sup>a</sup>, Samit Roy <sup>c</sup>, Ray H. Baughman <sup>b</sup>, Hongbing Lu <sup>a</sup>, \*

- <sup>a</sup> Department of Mechanical Engineering, The University of Texas at Dallas, Richardson, TX, 75080, USA
- <sup>b</sup> Alan G. MacDiarmid NanoTech Institute, The University of Texas at Dallas, Richardson, TX, 75080, USA
- <sup>c</sup> Department of Aerospace Engineering & Mechanics, University of Alabama Tuscaloosa, AL, 35487, USA

# ARTICLE INFO

# Keywords: MWNT sandwich composites Forest-drawn carbon multiwalled nanotube sheets Fracture toughness Cohesive zone modeling First-order shear deformation theory EMI shielding

# ABSTRACT

Strong, tough, and lightweight composites are increasingly needed for diverse applications, from wind turbines to cars and aircraft. These composites typically contain sheets of strong and high-modulus fibers in a matrix that are joined with other materials to resist fracture. Coupling these dissimilar materials together is challenging to enhance delamination properties at their interface. We herein investigate using a trace amount of carbon nanotube sheets to improve the coupling between composite skins and core in a composite sandwich. Ultra-thin (~100 nm) forest-drawn multi-walled carbon nanotube (MWNT) sheets are interleaved within the skin/core interphase, with MWNTs aligned in the longitudinal direction. The mechanical behavior is characterized by endnotched flexural testing (ENF). With two MWNT sheets placed in the skin/core interphase, the following performance enhancements are achieved: 36.8 % increase in flexural strength; 127.3 % and 125.7 % increases in mode I & II fracture toughness values, respectively; and 152.8 % increase in interfacial shear strength (IFSS). These are achieved with negligible weight gain of the composite sandwich (0.084 wt% increase over the baseline sandwich without MWNT sheets). The finite element simulation results show that MWNT sheets enhance the skin/core coupling by reducing stress concentration, enabling the transition from catastrophic brittle failure to a stable ductile failure mode. The MWNT sheets interleaved sandwich composites are thus demonstrated to be stronger and tougher while providing electrical conductivity  $(4.3 \times 10^4 \, \text{S/m})$  at the skin/core interface for potential de-icing, electromagnetic interference shielding, and structural health monitoring.

# 1. Introduction

Sandwich composites are lightweight structures with a desirably high strength-to-weight ratio and sufficient thickness to provide bending stiffness, the capability to carry a high bending moment, resist buckling, and offer high fatigue and dynamic performance [1–4]. They are used as structural elements that require low density, high strength, high stiffness, and long-term durability [5,6]. A composite sandwich structure consists of two composite skins (carbon fiber reinforced composites - CFRC, glass fiber reinforced composites - GFRC, aluminum sheets, etc.) bonded to a lightweight core (polyvinylchloride - PVC, polyethylene terephthalate - PET, polyurethane - PU, end-grain balsa, Nomex or aluminum honeycomb, etc.) [7,8]. The skin/core interphase is usually the most vulnerable region, and cracks usually initiate there [9]. Therefore, many researchers have made significant efforts to enhance

the interphase region to strengthen composite sandwich structures.

Numerous methods have been developed to enhance the skin/core interphase region in sandwich composites. These include using a nanopellet modified resin matrix [10], z-pinning [11], shear key insertion [12], core surface texturing [13], and interleaving a hybrid film [14] or a chopped fiber mat [15]. Using a nano-pellet-modified resin matrix is the most used method to enhance the skin/core bonding strength. Nano-pellet materials include carbon powders, carbon nanotubes (CNTs), graphene, metal powders, and non-metallic powders [16]. This nano-pellet route can enhance the fracture toughness of the skin/core interphase and provide enhanced impact, wear, and buckling resistance [17].

Z-pinning is another method for enhancing interphase mechanical performance. In this method, micro/nanofiber reinforcement is introduced in the liquid matrix in the skin/laminate, neighboring laminates,

E-mail address: hongbing.lu@utdallas.edu (H. Lu).

<sup>\*</sup> Corresponding author.

and skin/core interphase regions, then reoriented by electromagnetic or ultrasonic field to increase the stiffness in a particular direction. This method can increase the debonding strength in the skin/core interphase region and the adjacent fabric layers within the skin laminates. However, the micro/nano pins can potentially damage the fibers in the skins during the manufacturing process [18].

Shear key insertion is also a common way to enhance the properties in the skin/core interphase region [19]. Shear keys (carbon prepreg, metallic fibers, or bars) are inserted in the skin/core interphase region and in the core to enhance IFSS and increase the shear strength and stiffness of the core.

Another common method is to introduce surface texture to allow more resin to infuse into the interphase region to form an interlocking between core and skins, thereby increasing the fracture toughness of the skin/core interphase [7]. However, properly designing the texture patterns remains an area of exploration to further enhance the fracture toughness of the skin/core interphase [20].

Interleaving hybrid film or chopped fiber mats have recently received attention due to their ability to increase the skin/core interphase fracture toughness and flexural stiffness with a small weight gain compared with other approaches [21]. The mechanical properties of sandwich composites can be enhanced by incorporating synthesized hybrid films, which add multifunctionalities such as piezoelectricity [22,23], and magnetism [24,25].

Among various materials for enhancing the skin/core interphases, CNTs are often considered. CNTs have a high surface area (up to 1300 m<sup>2</sup>/g) and, therefore, low areal density, high modulus (up to 1 TPa), high strength (up to 150 GPa), high electrical conductivity ( $\sim 1 \times 10^7 S/$ *m*), and high thermal conductivity ( $\sim 3000 \ W/(m \bullet K)$ ) [26–29]. Carbon Nanotubes (CNT) have been utilized as an enhancement material in composites for aircraft, automotive, sports equipment, and marine structures [30]. It can enhance structural performance and provide multifunctional properties to the structure. A NASA report [31] indicated that the demand for multifunctional sandwich composites in aerospace applications will exceed conventional sandwich composites in 2030-2035. Numerous results demonstrated the benefits of using CNT as a nanofiller for composites. Jakubinek et al. found that using 1.0 wt% single-walled carbon nanotubes (SWNTs) in the epoxy resin matrix gives enhanced structural performance while providing electrical conductivity (reaching  $10^{-3}$ - $10^{-1}$  S/m) in the structural adhesive for fusion-joining aircraft components [32]. CNT-modified sandwich composites can also provide electromagnetic shielding (EMI shielding) and strain sensing for structural health monitoring and actuators, with performance reaching or exceeding that of copper in aerospace applications due to a large difference in strength-to-weight ratio between CNT and copper [33,34].

There are typically two ways to add CNTs to a sandwich composite: CNT dispersed in the polymer matrix and interleaving CNTs between fabric plies. In the CNT dispersion method, CNTs are dispersed into the resin, usually by sonication. Alak et al. found that 1.5 wt% MWNT introduced into the resin leads to a 14.4 % improvement in peak load under bending and a 34.34 % enhancement in mode I fracture toughness for a PVC foam core/GFRC skins sandwich composite [35]. M. Sánchez et al. determined that 0.1 wt% CNT in the resin leads to a 10 % improvement in flexural strength and 5.6 % enhancement in IFSS for the CFRC [36]. Han et al. introduced 0.1 wt% graphene oxide (GO) into the epoxy matrix and improved the ILSS by 8 % for the CFRC [37].

The second approach is interleaving MWNT sheets between the skin and core. Pratik et al. interleaved 2 MWNT sheets between two adjacent unidirectional carbon fiber plies at a small weight gain (0.016 wt%). The reported 49 % increase in flexural strength, 30 % ILSS enhancement, and 30 % improvement of mode I fracture toughness for the CFRC [38]. Zheng et al. investigated interleaving a 5 wt% CNT/polysulfide (PSF) hybrid film in a CFRC and obtained 53 % higher mode I fracture toughness, 34 % improvement of mode II fracture toughness, and 27 % and 29 % enhancement of flexural strength and modulus [39]. Li et al.

found that interleaving 30 layers of MWNT sheets in a CFRC leads to 90–110 % enhancement of the mode II fracture toughness under a low loading speed (8  $\times$  10 $^{-6}$  m/s) quasi-static loading and 20–30 % enhancement of the mode II fracture toughness under high loading speeds (8–16 m/s) [40]. Although the CNT dispersion method is considered state-of-the-art within composite structures communities, the potential for mechanical enhancement using CNTs merits further investigation, given their often discontinuous form within the matrix. Accordingly, exploring new processing methods for CNTs, such as densifying the Multi-Walled Nanotube (MWNT) sheet, represents the innovative focus of our research. Based on the available information, little research has been conducted on using a densified MWNT sheet (i. e., MWNT Xerogel) to provide performance improvements for sandwich composites. This paper is going to fill this research gap.

In this paper, composite end-notched sandwich specimens with MWNT sheets interleaved in the skin/core interphase region were fabricated by vacuum-assisted resin transfer molding (VARTM). The mode I and II fracture toughnesses, and energy absorption before catastrophic failure of the end-notched sandwich composites were measured by ENF testing. Crack initiation and propagation were observed by a high-speed camera. The surface principal strains around a crack tip were captured by digital image correlation (DIC).

The experimental results were analyzed using bi-layered first-order shear deformation theory and finite element method (FEM) simulations with a cohesive zone model. The IFSS, mid-span flexural strength, and mechanical energy absorption of the end-notched sandwich composite with two interleaved MWNT sheets were determined by FEM. A comparison with previous results is provided in the discussion section.

# 2. Methods

This section describes the procedures for preparing end-notched sandwich composite specimens with and without interleaved MWNT sheets in the skin/core interphase, experimental details and associated analyses, and the cohesive elements implemented in finite element modeling.

# 2.1. Materials

PVC foam (Divinycell<sup>TM</sup> H80-polyvinylchloride; Diab Group, DeSoto, TX), which is 25.4 mm thick, was used as the core of the lightweight sandwich structures. It was a waterjet cut to dimensions of  $203.2 \times 76.2 \times 25.4$  mm. Unidirectional glass fiber fabrics (UD 970; Saertex, LLC, Huntersville, NC) with an areal density of 957 g/m² and 1 mm densified thickness were used as the face sheets (aka skins). The MWNT sheets (1–4 plies) were laterally drawn from a chemical-vapor-deposition (CVD) grown 300- $\mu$ m-tall forest of about 10 nm outer diameter MWNTs (Lintec NSTC, Richardson, TX), which had high purity (>99%) and an areal density of approximately 0.025 g/m². These MWNT sheets were used as the interleaving sheets in the skin/core interphase [41].

Epoxy resin (EPIKOTE™ Resin MGS® RIMR 135) and curing agent (EPIKURETM Curing Agent MGS® RIMH 1366) from Westlake Epoxies Inc. (in Columbus, OH) were used in this work since they have relatively low viscosity at room temperature and can be cured at this temperature without developing entrapped bubbles. Two breathing films (Polyester; FibreGlast, Brookville, OH) and two release films (fluorinated ethylene propylene, also from FibreGlast) were used for each VARTM process. The stacking sequence on the mold surface was breathing film, release film, composite laminate, release film, and breathing film. A flowing media (low-density polyethylene, again from FibreGlast) was placed between a breathing film and a release film to improve resin flow in the vacuum bagging film. Teflon tape and a mold release agent (FibRelease®) from FibreGlast generated an interfacial crack between the skin and core in the end-notched sandwich composite specimen. The materials were stored, fabricated, and tested under controlled conditions at room temperature and 25 % relative humidity to eliminate external

factors affecting the testing results.

### 2.2. Preparation of end-notched sandwich composite specimens

We next describe the method used to prepare the end-notched composite sandwich specimen to measure skin/core interfacial strength. Fig. 1 shows a schematic diagram for preparing the MWNT sheets interleaved PVC foam core/glass fiber face sheet sandwich composites.

Several MWNT sheets and Teflon tapes were first placed in a sequence as shown in Fig. 1. The Teflon tapes were placed over the MWNT sheets by 50.8 mm, then the mold release agent was sprayed on the Teflon taped region to generate a sufficient debonding around the

crack tip. Afterward, MWNT sheets were laid down on the smooth side of the H80 PVC foam core. Next, ethanol was sprayed on the MWNT sheets to densify the MWNT sheets into a densified MWNT film. The composite skins were made of 2 layers of glass fiber fabrics on each side. Next, breathing cloth, release film, glass fiber fabric, modified PVC foam, glass fiber fabric, release film, and breathing cloth were laid in order. Materials used for the sandwich composites are shown in Fig. 2.

Later, the entire laminate was covered by a vacuum bagging film (Nylon; FibreGlast) and sealed with sealant tape (Yellow tape; FibreGlast). Then, the epoxy resin mixture (degassed at  $20\,^{\circ}C$  for 30 min) was transferred to the laminate. Next, the vacuum was applied for 2 h until the epoxy mixture infiltrated the entire sandwich structure at room temperature. Finally, the vacuum-bagged sandwich composite was

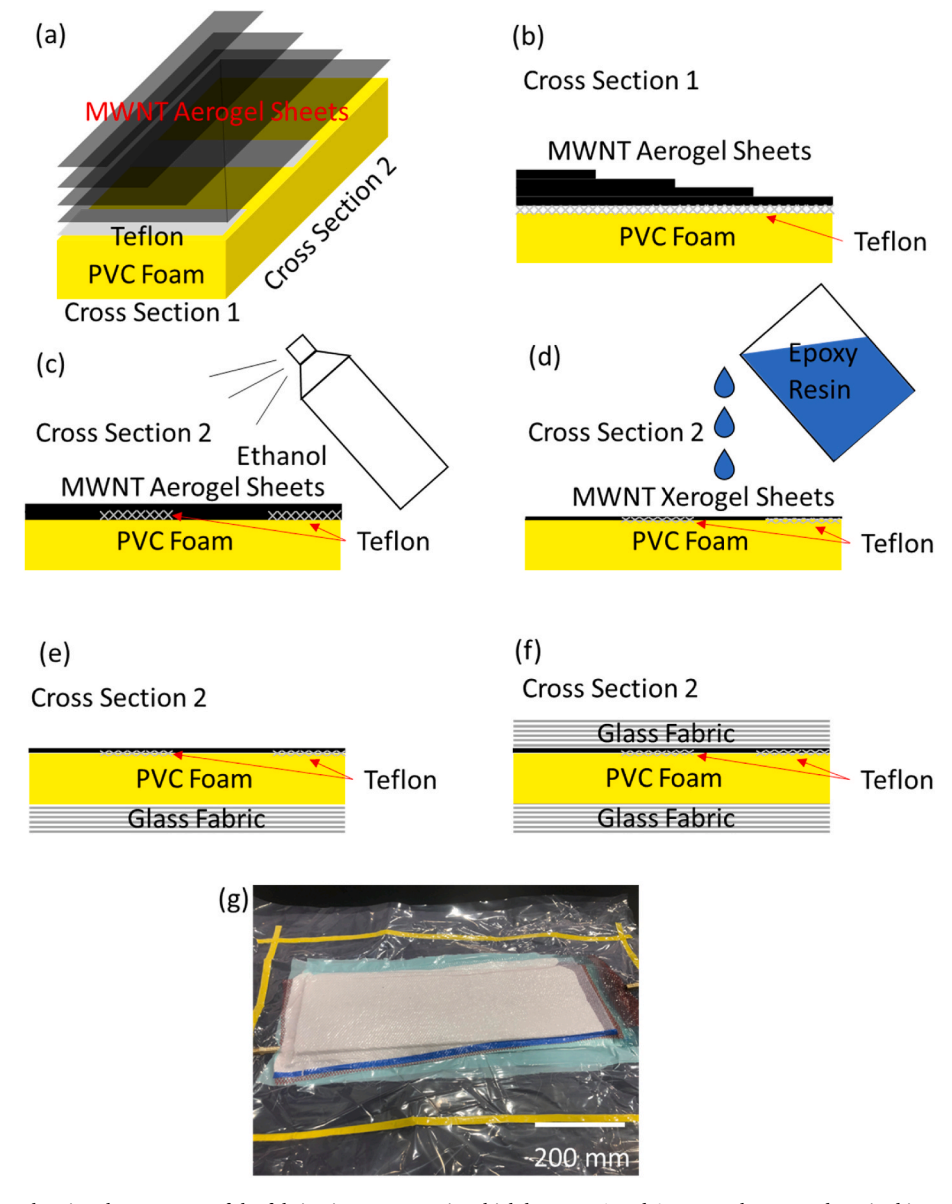


Fig. 1. Schematic diagrams showing the sequence of the fabrication processes in which between 1 and 4 MWNT sheets are deposited in a patterned manner on top of sacrificial Teflon tapes, these MWNT layers are liquid-evaporation densified while attached to a PVC foam, these MWNT sheets are then resin infiltrated; finally, the outer glass fiber fabric skins are attached to the MWNT and PVC foam stacks: (a) 3D schematic of the MWNT sheets/Teflon tapes coated PVC foam, sequence: Teflon tapes overlayed on a PVC foam sheet, following 1 layer to 4 layers of MWNT sheet interleaved on PVC foam, (b) 2D cross sectional view of the MWNT sheets/Teflon tapes coated PVC foam, (c) MWNT sheets interleaved PVC foam densified by ethanol, (d) a densified MWNT sheet coated PVC foam impregnated by resin droplets, (e) 2 layers of glass fabrics overlayed on the bottom side of densified MWNT sheet coated PVC foam, (g) a general view of VARTM setup (resin flow: right-hand side to left-hand side, composite laminate in-plane dimensions: 812.8 × 304.8 mm, VARTM setup overlaying schedule: (from top to down) breathing cloth-flow media-release film-composites-release film-flow media-breathing cloth-mold).

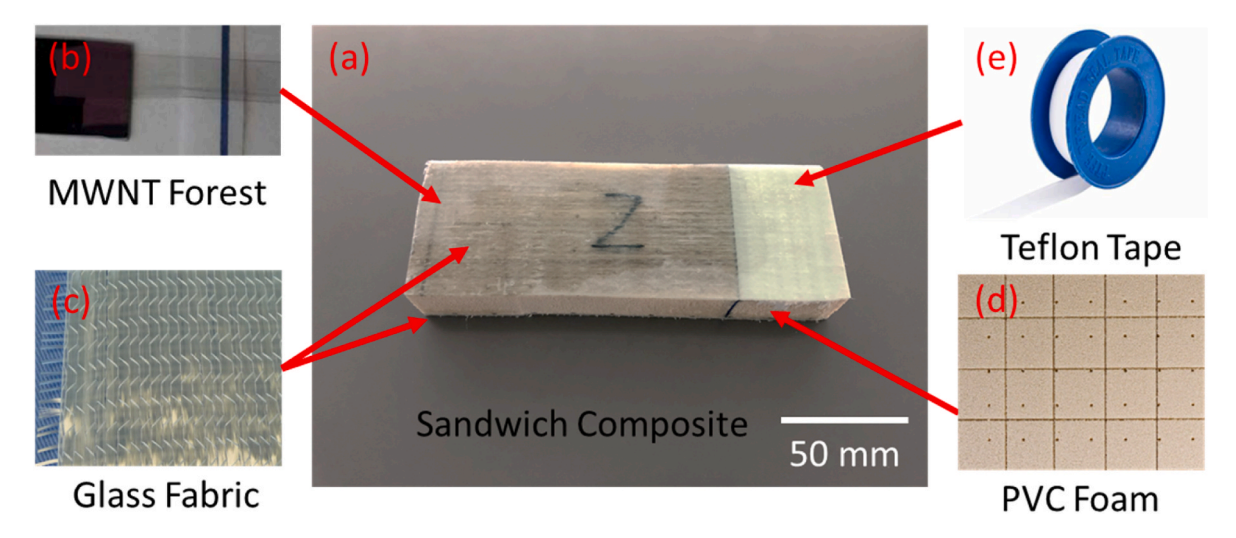


Fig. 2. Two layers of MWNT sheets interleaved end notched GFRC skin/H80 GPC PVC foam core sandwich composite prepared by the VARTM process: (a) an MWNT sheets modified sandwich composite; (b) an MWNT sheet laminated from an MWNT forest; (c) a unidirectional glass fabric; (d) a PVC foam panel; (e) a Teflon tape.

placed in an oven and cured at 80 °C for 4 h.

# 2.3. ENF testing

Following the ASTM D7905 standard [42], the delamination properties of the sandwich composites at the skin/core interface were measured by the End-Notched Flexure (ENF) testing, as illustrated in Fig. 3. A support span-to-depth ratio of 6:1 was used. Values of 4:1, 5:1, and 6:1 were also used to determine the effect of aspect ratio. A 50.8 mm pre-crack was generated by the Teflon tapes for each sandwich composite. The specimen dimensions were 203.2  $\times$  76.2  $\times$  25.4 mm. The H80 grooved and perforated (GPC) PVC foam core was selected due to its lightweight and closed-cell structure. Five types of specimens were prepared: baseline, 1 MWNT sheet, 2 MWNT sheets, 3 MWNT sheets, and 4 MWNT sheets, and three specimens were tested for each type of sandwich composite. Mid-point deflection and bending load on an Instron 5969 material test system were recorded, and the flexural properties were calculated. The crosshead speed was set as 0.5 mm/min to obtain stable debonding at the skin/core interphase. All the tests were carried out successfully, and the effect of MWNT sheets was systematically investigated. Three tests were conducted for each case to ensure repeatability of the testing results.

# 2.4. Surface strain measurement by DIC

The DIC technique, a non-contact full-filed deformation measurement method [43–46], was used to measure the deformations of the side surface of a specimen using a commercially available 2D GOM Correlate software (GOM Inc., Charlotte, NC). During an ENF test, digital images of the specimen surface were acquired every 5 s using a Nikon D7100 camera with  $3840 \times 2748$  pixels resolution and a 40-mm lens. The work distance of the lens was 1.9 m, which allowed us to capture images of the entire support span of the specimen within the region of interest.

# 2.5. Image acquisition by a high-speed camera

A FASTCAM SA6 high-speed camera system was used to acquire surface images that enabled observation of the high-speed events for crack initiation and propagation. The camera had a resolution of  $1280 \times 1024$  pixels and could record motion up to 20,000 frames/s and store up to 5000 full frames in memory. A NiLA VARSA LED light was used for illumination. A frame rate of 2000 frames/s was used in experiments. Image visualization was made using FASTCAM Viewer (PFV) software (V6.4).

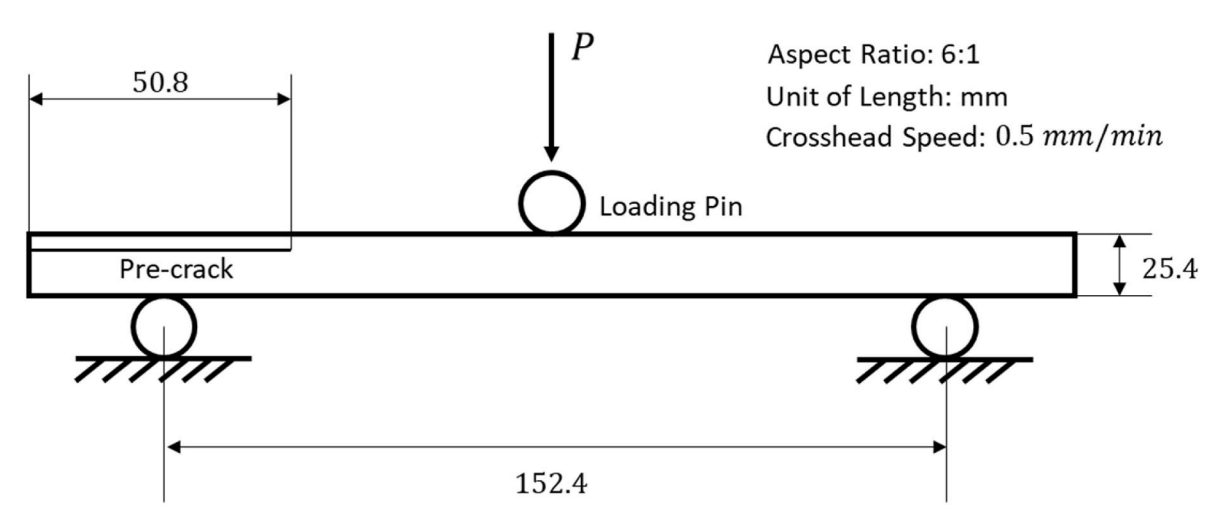


Fig. 3. A schematic diagram of ENF testing of a composite sandwich specimen.

# 2.6. Measurement of electrical conductivity

The electrical conductivity of the two MWNT sheets modified sandwich composites (50.8  $\times$  50.8  $\times$  30.5 mm) along the longitudinal direction was measured using a DC power supply. A BK-precision model 9202 power source at 15 V was used to measure the electrical resistance. In conjunction with a conductive silver paste, copper sheets were applied at the contact region of MWNT and copper sheets to reduce the wire resistance and increase the contact area. The electrical conductivity was calculated from the measurement with the consideration of the specimen dimensions.

# 2.7. Finite element modeling implementing a CZM

A finite element model implementing a CZM in the skin/core interphase region was used to simulate the skin/core debonding behavior of the end-notched sandwich composites at 6:1 aspect ratio in Abaqus 6.14 explicit code [47]. 4-node bilinear plane stress quadrilateral elements (type: CPS4R) were used for skin, core, and loading pins. Reduced integration and hourglass control techniques were used to achieve faster convergence. In the skin/core interphase region, 4-node two-dimensional cohesive elements (type: COH2D4) were used to simulate debonding. The total number of elements in the adaptive mesh was  $1.5 \times 10^5$  to eliminate the mesh dependence for simulations of steady crack propagation in the skin/core interphase region. A thin cohesive layer (baseline) with a thickness of 15 um, determined by microscopic observation, was introduced in the end-notched skin/core interphase region of the specimen to model the bonding between the skin and core by epoxy. However, due to a high stiffness in the 2 MWNT sheets enhanced skin/core interphase region, the usage of CZM elements encountered difficulty in achieving convergence. Both CZM elements and 4-node bilinear plane stress quadrilateral elements implementing ductile damage criterion with exponential softening behavior were used in the simulations of the 2 MWNT sheets interleaved skin/core interphase region to resolve this issue. Hill's yielding criterion was used in the 2 MWNT sheets interleaved sandwich composite skins region simulations. Compared with the conventional Cohesive Zone Model (CZM) for simulating debonding behavior in the sandwich composites' interphase, this model offers significantly faster convergence and higher accuracy, especially for simulating a step change in the stiffness of the skin/core interphase region. Additional details are provided in the results and discussion section.

The flexural stress, in-plane shear strain, and IFSS distributions for the end-notched sandwich composites were visualized in the front view, zoom-in view at the crack tip, and zoom-in view at the loading pin. The energy absorption of the end-notched sandwich composites is reported in the results and discussion section.

Mechanical properties and cohesive parameters of the end-notched sandwich composite are listed in Tables 1 and 2.

The fracture parameters used in the quadrilateral and CZM elements are listed in Table 2. The Young's modulus of MWNT interleaved skin/core interphase ( $E_{in}=130$  GPa) was determined by matching the load-deflection curves to the experimental data. The Young's modulus of the skin/core interphase region was determined as 130 GPa, which is 36 times higher than that of the cured epoxy ( $E_r=3.6$  GPa) [48]. We considered that the skin/core interphase thickness is equal to that of the baseline and 2 MWNT sample model in FEM. Although we are using the

same type of glass fabric and core, the actual thickness of the skin/core interphase region can be different because of the inconsistency in the surface textures of the glass fabric skin and cellular microscale topography of the foam core.

# 2.8. Extraction of the thickness and Young's modulus in the skin/core interphase region using an inverse method

Based on the rule of mixtures, Young's modulus of the skin/core interphase region is

$$E_{i\_rom} = \left( E_{MWNT} t_{MWNT} + E_r t_r \right) / t_i \tag{1}$$

Here, t indicates the thickness of the material. Subscript MWNT, r and i are denoting the MWNT layer, resin layer, and skin/core interphase. The Young's modulus of MWNTs is taken as 1 TPa [50].

From the curve fitting method, the Young's modulus of skin/core interphase region is

$$E_{i \to fit} = f\left(E_{fit}, I_{fit}\right) / I_i = E_{fit} \bullet t_{fit}^3 / t_i^3$$
(2)

Here  $f(E_{fit}, I_{fit})$  is a numerical constant (flexural rigidity of skin/core interphase region:  $E_{fit} \bullet I_{fit} = 3.1 \times 10^{19}~GPa \bullet \mu m^4$ ) which follows the Euler–Bernoulli beam theory (EBT) in the FEM. When the flexural rigidity of the skin/core interphase region remains constant in the composite structure, the stiffness of the sandwich composite should also stay the same as an arbitrary skin/core interphase thickness.

The skin/core interphase thickness is

$$t_i = t_{MWNT} + t_r \tag{3}$$

Fig. 4 shows Young's modulus and stiffness of the two layers of MWNT interleaved skin/core interphase end-notched sandwich composite as a function of interphase thickness.

Properly defining the thickness and Young's modulus of the skin/core interphase region of the MWNT sheets interleaved end-notched sandwich composite in the FEM is challenging. Based on the rule of mixture, Young's modulus of the skin/core interphase region should be close to the cured epoxy ( $E_r=3.6$  GPa) due to a massive thickness difference between the cured epoxy layer (15–50  $\mu$ m) and densified MWNT layer (~200 nm). When we define a thin layer with the solid element as the MMWNT-modified skin/core interphase in FEM, Young's modulus acquired from the curve fitting method is higher than the rule of the mixture method. The intersecting point between the two curves ( $E_{i\_fit}$  and  $E_{i\_rom}$ ) are (95  $\mu$ m, 5.60 GPa). Theoretically, the intersecting point should give the realistic material behavior if Young's modulus in the MWNT sheets interleaved skin/core interphase region following the rule of the mixer.

However, based on the information in Fig. 4b, the stiffness of the MWNT sheets interleaved end-notched sandwich composite is no longer realistic when the skin/core interphase is  $> 50~\mu m$  in the FEM. Because the moment of inertia of the skin/core interphase contributes to the flexural rigidity, no longer Young's modulus. So, achieving a reasonable stiffness ( $<50~\mu m$ ) is impossible under the setting of 95  $\mu m$  and 5.60 GPa in the FEM. Furthermore, based on the information in Fig. 4, it is still unclear whether the MWNT interleaved skin/core interphase is following the rule of mixer or the FEM is unrealistic.

**Table 1**The elastic properties of the UD970 glass fiber/epoxy composite skin and the H80 PVC foam core [35].

Material	$E_1$	$E_2$	$E_3$	$\nu_{12}$	$\nu_{13}$	$\nu_{23}$	$G_{12}$	$G_{13}$	$G_{23}$
UD970 glass/epoxy skin	32 GPa	19 GPa	19 GPa	0.32	0.32	0.32	12.3 GPa	12.3 GPa	7.3 GPa
H80 PVC foam core	98 MPa	55 MPa	55 MPa	0.34	0.349	0.207	28 MPa	28 MPa	19 MPa

Note: Subscript 1 indicates the longitudinal direction, and subscripts 2 and 3 indicate transverse directions. The units for the properties of the UD970 glass skin and the H80 PVC foam core are *GPa* and *MPa*, respectively.

**Table 2**Fracture parameters used in the quadrilateral and CZM elements.

Specimen	Region	K (N/mm)	E (GPa)	$\sigma_f$ (MPa)	$d_f$ ( $mm$ )	η	$\varepsilon_f$ (mm/mm)	ST (MPa/MPa)	$\dot{arepsilon}_r$ (mm/mm/min)
Baseline	end-notched skin/core interphase	10 <sup>6</sup>	_	29	0.13	$10^{-5}$	_	_	_
	skin/core interphase	$10^{6}$	_	115	0.13	$10^{-5}$	_	_	_
2 MWNT sheets	end-notched skin/core interphase	$10^{6}$	_	12	0.6	$10^{-5}$	_	_	_
	skin/core interphase	_	130	_	0.1/n = 10	_	$8  imes 10^{-4}$	1	0.02

Note: K: cohesive stiffness [49], E: Young's modulus,  $\sigma_f$ : local stress at the fracture initiation point,  $d_f$ : local displacement at failure; n: exponential term,  $\eta$ : viscous regulation term,  $\varepsilon_f$ : local fracture strain at the fracture initiation point, ST: stress triaxiality,  $\dot{\varepsilon}_r$ : strain rate at the fracture initiation point.

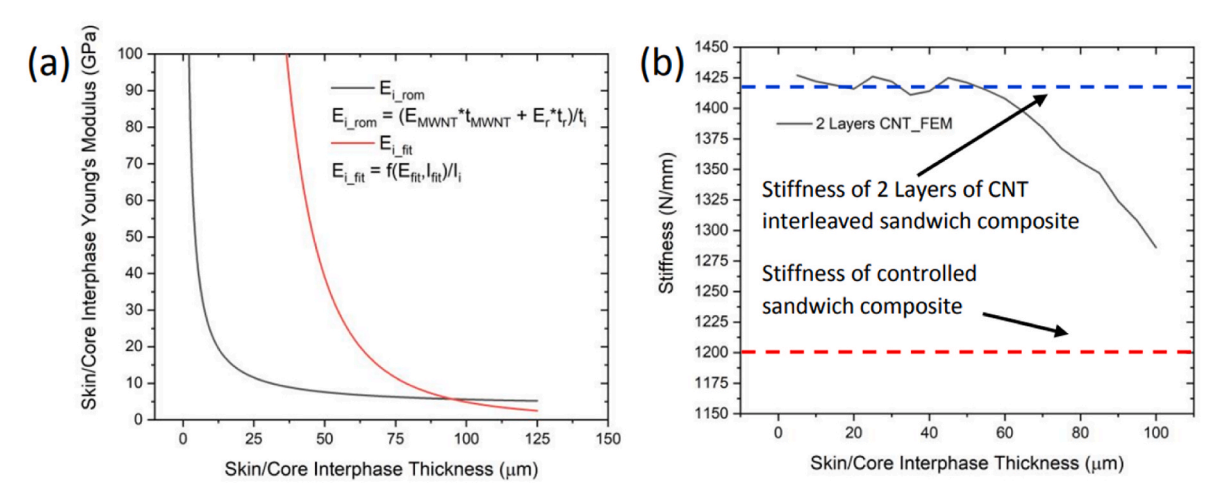


Fig. 4. The Young's modulus and stiffness of the two layers of MWNT interleaved skin/core interphase end-notched sandwich composite as a function of interphase thickness: (a) Young's modulus of skin/core interphase region; (b) stiffness of the end-notched sandwich composite.

# 3. Analytical approach for mode I and II fracture toughnesses and stress intensity factors

The first-order shear deformable bi-layer beam theory is used to derive mode I and II fracture toughnesses of a sandwich composite under the ENF test proposed by Wang et al. [51]. The advantage of this theory lies in its ability to distinguish between Mode I and II fracture toughness values from the ENF test. It has also been utilized by several researchers in studying functionally graded beams, where mechanical properties change across the thickness [52–55]. The intermediate derivation steps are shown in the SI section. All the parameters were defined in Appendix A Table A1 of the SI section.

The expressions for mode I and II fracture toughnesses are given as,

$$G_{I} = 0.5 \left(\frac{1}{B_{t}} + \frac{1}{B_{b}}\right) \left[V + k(M + \frac{h_{t}N}{2})\right]^{2}$$
 (1)

$$G_{II} = \frac{1}{h_1 \xi + 2\eta} (\xi M - \eta N)^2$$
 (2)

Here, M, N, and V are the internal bending moment, axial force, and shear force, respectively. k,  $\xi$ , and  $\eta$  are parameters in the tangential stiffness matrix.  $B_t$  and  $B_b$  are the shear stiffness coefficient term of the global stiffness matrix for the top and bottom layer of the sandwich composite.  $h_t$  is the thickness of the top layer of sandwich composite.

Hwu et al. investigated [56] the mixed-mode fracture in a bi-layer sandwich beam using the first-order deformation shear theory under the plane stress condition. The relationships between mode I and II fracture toughnesses and stress intensity factors for the ENF specimen are

$$G_I = \frac{K_I^2}{4} \tag{3}$$

$$G_{II} = \frac{K_{II}^2}{4} \tag{4}$$

# 4. Results and discussion

# 4.1. Characterization of the mode II fracture behavior of sandwich composite under ENF test

We herein report the experimental results obtained in experiments. The numerical results for the effect of MWNT sheets and aspect ratio are listed in Table 3.

The densification conditions and failure modes of the MWNT interleaved sandwich composites are shown in Fig. 5. The results indicate that the MWNT was properly densified on the PVC foam core surface and successfully enhanced the delamination toughness of the sandwich composites.

From Fig. 5(a) and (b), the densification process can successfully elapse the pores in the MWCNT sheets. However, the densification process can create knots and wrinkles between the MWCNT bundles owing to the surface tension of ethanol droplets. So, properly controlling the amount of ethanol applied to the MWCNT sheets is critical to secure the enhancement performance of sandwich composites. In Fig. 5(c) and (d), the failure mode changes from skin/core interphase debonding into core shearing failure. Inducing two layers of MWNT sheets in the skin/core interphase successfully enhanced the debonding toughness of the sandwich composite.

The geometries of the crack initiation are shown in Fig. 6. Based on the four subfigures of Fig. 6, the geometry of the crack initiation path is not straight. The effective crack length for fracture initiation for the MWNT sheets interleaved end-notched sandwich composites (1, 2, 3, and 4 MWNT sheets interleaved) is 2.4 mm, 2.6 mm, 1.4 mm, and 2.3 mm, respectively. Under 2000 *fps* used in observation, the camera could

 Table 3

 A summary of the effect of MWNT sheets and aspect ratio on debonding load capacity and debonding stiffness in the end-notched sandwich composite specimens.

Number of MWNT sheets	Initial crack length (mm)	Aspect ratio	Debonding load (N)	Load enhancement (%)	Debonding stiffness ( <i>N/mm</i> )	Debonding stiffness variation (%)
Baseline (0)	50.8	6:1	2856.47	_	1269.83	_
1			2888.60	1.12	1248.84	_
2			3908.62	36.83	1395.46	9.89
3			3265.35	14.31	1413.20	11.29
4			2952.60	3.37	1244.47	_
2		5:1	3005.86	_	1427.97	2.33
2		4:1	3747.01	_	2317.45	66.07

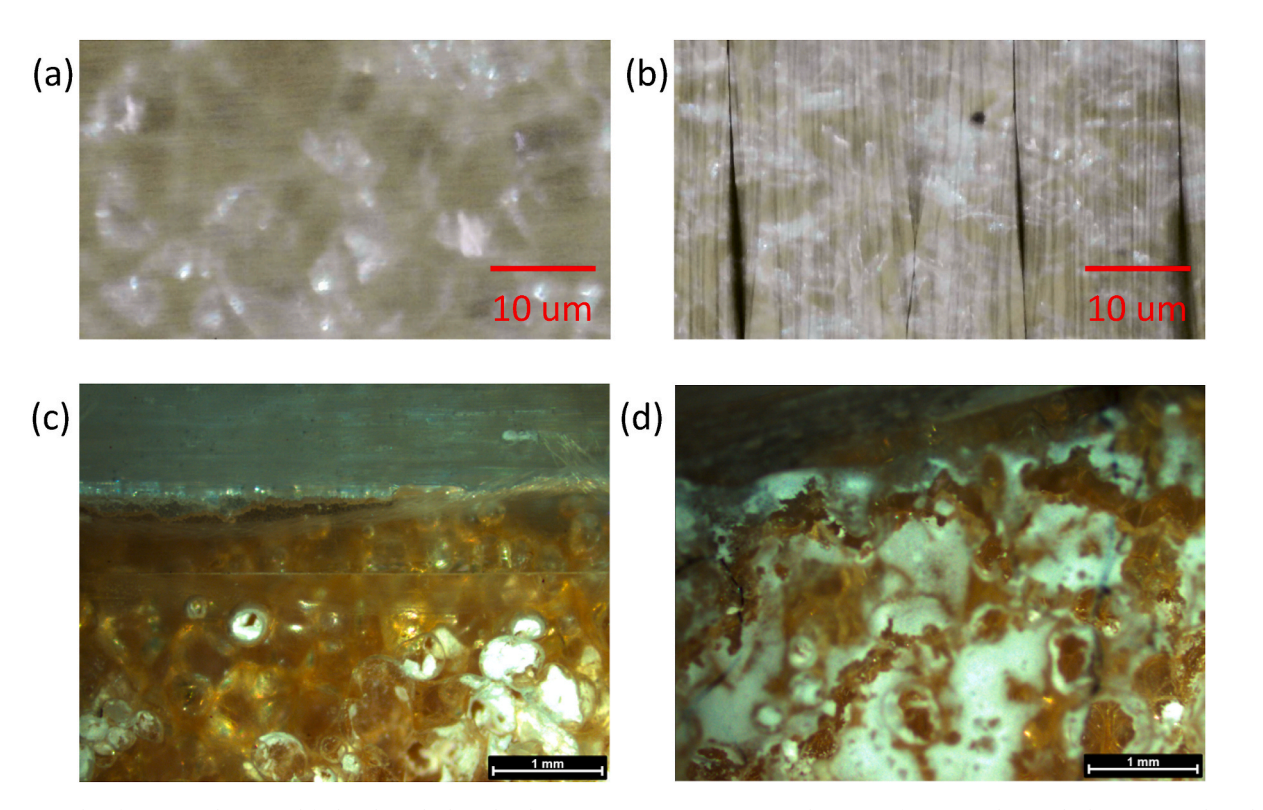


Fig. 5. Micrographs of MWCNT sheets modified end-notched sandwich composites: (a)  $40 \times \text{magnitude}$  image of MWCNT sheets which were coated on the PVC foam, (b)  $40 \times \text{magnitude}$  image of MWCNT sheets which was coated then densified on the PVC foam, (c)  $5 \times \text{magnitude}$  fractographic image of the baseline sample, (c)  $5 \times \text{magnitude}$  fractographic image of the 2 MWCNT sheets interleaved sample.

not capture the images showing the crack initiations in these ENF specimens.

# 4.2. Analysis of the mode I and II fracture of the sandwich composite under ENF test

The mode I and II fracture toughness (G) was directly acquired from load versus deflection curves (Fig. 3a in SI) under ENF tests through energy release (U) with unit incremental crack length ( $\Delta a$ ) (expression:  $G=-\frac{1}{b}\frac{dU}{da}$ ). The mode I and II fracture toughnesses (GI and GII) and stress intensity factors (KI and KII) are obtained by equations in section 3 eqs (1)–(4). The effect of MWNT sheets on the fracture propagation of the MWNT sheet interleaved sandwich composite under ENF tests is shown in Fig. 7. MWNT enhances the fracture toughness of sandwich composite skin/core interphase by reinforcing the local stiffness (MWNT reinforcement location: right above the core surface), thereby improving load transfer between the skin and core, and delaying crack initiation and propagation in the skin/core interphase.

From Fig. 7a, mode I fracture toughness ( $G_I$ ) at the 2nd fracture initiation stage (a=50.8 mm) for the baseline, 1 MWNT sheet interleaved, 4 MWNT sheets interleaved, 2 MWNT sheets interleaved, 2

MWNT sheets interleaved specimens are 0.11 kJ/m<sup>2</sup>, 0.11 kJ/m<sup>2</sup>, 0.12 kJ/m<sup>2</sup>, 0.17 kJ/m<sup>2</sup>, and 0.25 kJ/m<sup>2</sup>, respectively. Compared with the baseline specimen, the mode I fracture toughness (GI) at the fracture initiation stage for the 2 MWNT sheets interleaved specimen was enhanced by 127.3 % for the ENF test. The mode I fracture toughness  $(G_I)$  at 2nd fracture end-stage (a = 76.2 mm) for the baseline, 1 MWNT sheet interleaved, 4 MWNT sheets interleaved, 3 MWNT sheets interleaved, 2 MWNT sheets interleaved specimens are 0.71 kJ/m<sup>2</sup>, 0.74 kJ/ m<sup>2</sup>, 0.77 kJ/m<sup>2</sup>, 0.94 kJ/m<sup>2</sup>, and 1.35 kJ/m<sup>2</sup>, respectively. Compared with the baseline specimen, the mode I fracture toughness (GI) at the 2nd fracture end-stage for the 2 MWNT sheets interleaved specimen was enhanced by 90.1 % under the ENF test. So, under the mode I fracture, interleaving the MWNT sheets in the skin/core interphase region will see greater toughness enhancement for fracture initiation than for crack propagation. crack propagation. The primary reason for providing higher benefit to fracture initiation than when the crack propagated to a certain depth along the skin/core interphase region ( $\Delta$  a = 24–25 mm) is due to the difference in the strain rate involved in the loss of structural stability. As the crack continues to propagate within the skin/core interphase of a sandwich structure, its propagation speed decreases, and so does the strain rate, whereas, at crack initiation, a high strain rate is involved, where the enhancement in crack initiation fracture toughness

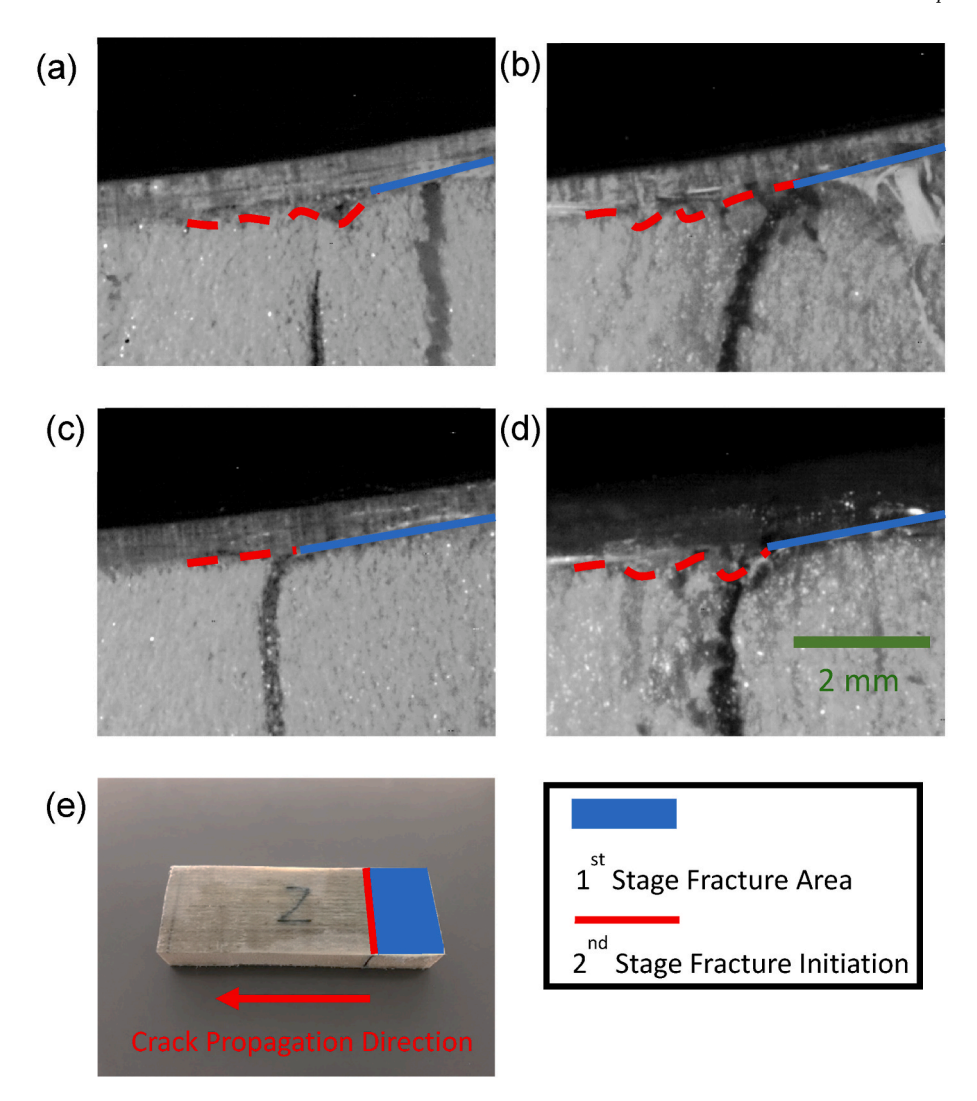


**Fig. 6.** High-speed images showing the 2nd stage crack initiation on top skin/core interphase of the MWNT sheet interleaved sandwich composite (frame rate: 2000 fps): (a) ENF sandwich composite specimen with one layer of MWNT sheet interleaved, (b) ENF sandwich composite specimen with two layers of MWNT sheets interleaved, (c) ENF sandwich composite specimen with four layers of MWNT sheets interleaved, (e) a schematic diagram of 1st and 2nd fracture stages of ENF sandwich composite specimen.

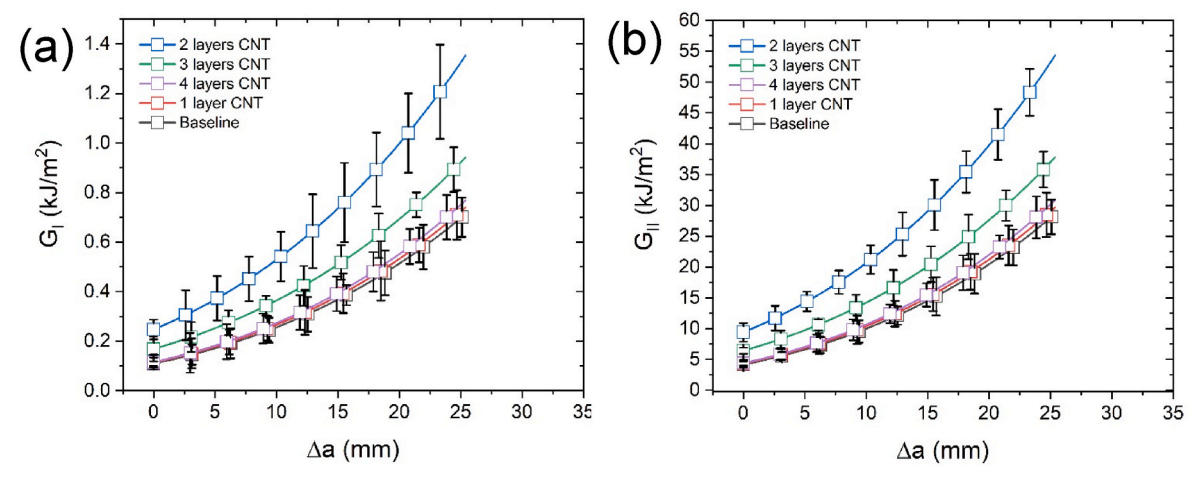


Fig. 7. Effect of MWNT sheets on the fracture toughness of the MWNT sheets interleaved sandwich composite under ENF test: (a) mode I fracture toughness ( $G_{I}$ ) versus crack extension, (b) mode II fracture toughness ( $G_{II}$ ) versus crack extension. (Initial crack length: 50.8 mm)

is more pronounced. The MWNT interleaved interphase plays a less significant role in preventing failure due to the type of catastrophic failure observed in sandwich structures toward the end of testing ( $\Delta$  a >25 mm), which is not limited to debonding between the skin and core, as the crack propagates into the foam region as well.

The mode II fracture toughness ( $G_{II}$ ) at the 2nd fracture initiation stage (a=50.8~mm) for the baseline specimen and 2 MWNT sheets interleaved specimens are  $4.17~\text{kJ/m}^2$  and  $9.41~\text{kJ/m}^2$ , respectively. The mode II fracture toughness ( $G_{II}$ ) at the 2nd fracture end-stage (a=76.2~mm) for the baseline specimen and 2 MWNT sheets interleaved specimens are  $28.61~\text{kJ/m}^2$  and  $54.34~\text{kJ/m}^2$ , respectively. Compared with the baseline specimen, the mode II fracture toughness ( $G_{II}$ ) at the 2nd fracture initiate and end-stage for the 2 MWNT sheets interleaved specimen were enhanced by 125.7 % and 89.9 % under the ENF test, respectively. Generally speaking, under the ENF boundary condition, an ENF sandwich composite specimen with two layers of MWNT sheets interleaved on the skin/core interphase shows the best skin/core debonding enhancement. The MWNT sheets show a consistent percentage enhancement in mode I and mode II fracture toughness (G) over the baseline case.

The mode I stress intensity factor (K<sub>I</sub>) at 2nd fracture initiation stage (a = 50.8 mm) for the baseline specimen and 2 MWNT sheets interleaved specimen are 0.13  $MPa\sqrt{mm}$  and 0.19  $MPa\sqrt{mm}$ , respectively. Compared with the baseline specimen, the mode I stress intensity factor (K<sub>I</sub>) at the fracture initiate stage for the 2 MWNT sheets interleaved specimen was enhanced by 46.2 % under the ENF test. The mode II stress intensity factor ( $K_{II}$ ) at the fracture initiation stage (a = 50.8 mm) for the baseline specimen and 2 MWNT sheets interleaved specimen are 0.80  $MPa\sqrt{mm}$  and 1.20  $MPa\sqrt{mm}$ , respectively. Compared with the baseline specimen, the mode II stress intensity factor (K<sub>II</sub>) at the fracture initiate stage for the 2 MWNT sheets interleaved specimen was enhanced by 50.0 % under the ENF test. The highest enhancement in toughness observed in specimens with 2 MWNT sheets interleaved, compared to those with 1, 3, and 4 MWNT sheets, is attributed to the optimal amount of Xerogel applied in the skin/core interphase. An excessive amount of Xerogel is prone to shear cracking in the CNT Xerogel sheets plane under load, as the CNT sheets can easily slide against each other, and become brittle, thus reducing the interphase's ductility, energy absorption, and overall toughness [57,58]. Furthermore, Alessandro et al. [59] have noted the critical role of the distance between two MWNT sheets in affecting sliding force, or in another term, the Interfacial Shear Strength (IFSS). When the gap is less than 0.34 nm, the sliding force increases exponentially as the distance decreases due to a linear increase in van der Waals traction. During the sliding stage of the MWNT sheet, the external force applied transitions from kinetic to potential energy, facilitated by van der Waals traction between the sheets. This stored potential energy enhances energy absorption, thereby delaying fracture initiation in the skin/core interphase of the sandwich structure.

During the ENF tests, we modified the ratio of Mode I to Mode II fracture toughness values by altering the aspect ratio and the loading position within the supporting region. Our goal was to assess Mode II fracture toughness and energy absorption. We utilized an aspect ratio of 6:1 under central loading. Subsequent analysis of the raw data was conducted using the bi-layered first-order shear deformation theory, which enables us to differentiate between Mode I and Mode II fracture toughnesses. The mode I fracture toughness (G<sub>I</sub>) at the 2nd initiation stage for baseline and 1-4 MWNT sheets interleaved specimens are 0.11 kJ/m<sup>2</sup>, 0.12 kJ/m<sup>2</sup>, 0.25 kJ/m<sup>2</sup>, 0.17 kJ/m<sup>2</sup>, and 0.12 kJ/m<sup>2</sup>, respectively. At the 2nd fracture initiation stage, when 2 MWNT sheets interleaved in the skin/core interphase region of the sandwich composite, the mode II fracture toughness (G<sub>II</sub>) is enhanced by 110.32 %, as shown in Fig. 8. Since the percentage enhancement of fracture toughness (G) is higher than the stress intensity factors (K), the crack propagates should slowly along the skin/core interphase. This conclusion is consistent with the experimental investigation. Although 1 MWNT sheet interleaved

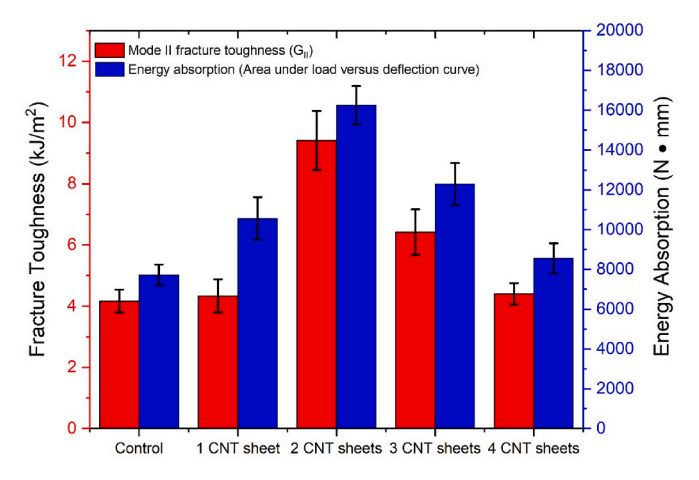


**Fig. 8.** The effect of the number of MWNT sheets inserted in the skin/core interphase region on the 2nd stage crack initiation mode II fracture toughness  $(G_{II})$  and mechanical energy absorption under the mixed mode fracture condition of the MWNT sheet interleaved sandwich composite in ENF testing. Note: The 2nd stage fracture initiation triggers at the peak flexural stress stage, and the crack propagates to the MWNT interleaved interphase. Due to a massive difference between the mode I and II fracture toughnesses  $(G_I \& G_{II})$ , the mode I fracture toughness  $(G_I)$  is not shown in this figure.

end-notched sandwich composites do not significantly enhance the mode I and II fracture toughnesses ( $G_I \& G_{II}$ ), the fracture toughness ( $G_I$ ) increases due to the inserted MWNT sheets. Also, from Fig. 6a and b, the crack propagation speed is reduced with increased fracture toughness ( $G_I$ ). At the second fracture initiation stage, introducing MWNT sheets into the skin/core interphase enhances stiffness, including at the crack tip. This enhancement reduces the shear stress levels at the crack tip, thereby delaying fracture initiation and increasing both fracture toughness and energy absorption. A detailed analysis of the crack tip was performed using FEM, the results of which are illustrated in the figures that follow.

In Fig. 9a, the 2 stages of fracture initiation of the MWNT sheets interleaved, and baseline sandwich composites are successfully captured through the IFSS on the crack tip. However, the 1st stage fracture initiation of the baseline specimen does not affect the stress state too much due to a weak bonding on the end-notched region. For the MWNT sheets interleaved specimen, 1st stage fracture initiates at 32.6 MPa and then gradually decreases to 20.3 MPa within  $\sim$ 2.6 mm. When the 1st stage fracture finishes crack propagation, the interfacial shear stress climbs back to 41.6 MPa within  $\sim$ 0.5 mm, and a sinusoidal stress wave arises with initially  $\sim$ 2.6 MPa amplitude with a period of  $\sim$ 1.2 mm. After 5 sinusoidal stress waves, the interfacial shear stress stabilizes at 42.9 MPa until the 2nd stage fracture initiation occurs. The sinusoidal stress (Amplitude: ~17.2 MPa, period: ~0.5 mm) waves arise again after the 2nd stage fracture is triggered. For the baseline specimen, the stress field in front of the crack tip is also sinusoidal in form with an irregular amplitude and period. However, a higher computational cost is needed for a detailed sinusoidal stress state around the crack tip. Fig. 9a shows a general interfacial shear stress trend around the crack tip during the crack propagation in the MWNT sheets interleaved skin/core interphase region, which balances the computational cost and numerical accuracy. The MWNT sheet's interleaved skin/core interphase plays a significant role in preventing fracture initiation under the loading pin region since the loading pin applies the compression load directly to the glass skin without exceeding the skin loading capacity. In addition, this mechanism also works on the core material under the loading pin to prevent the local core from crushing under the compression loads.

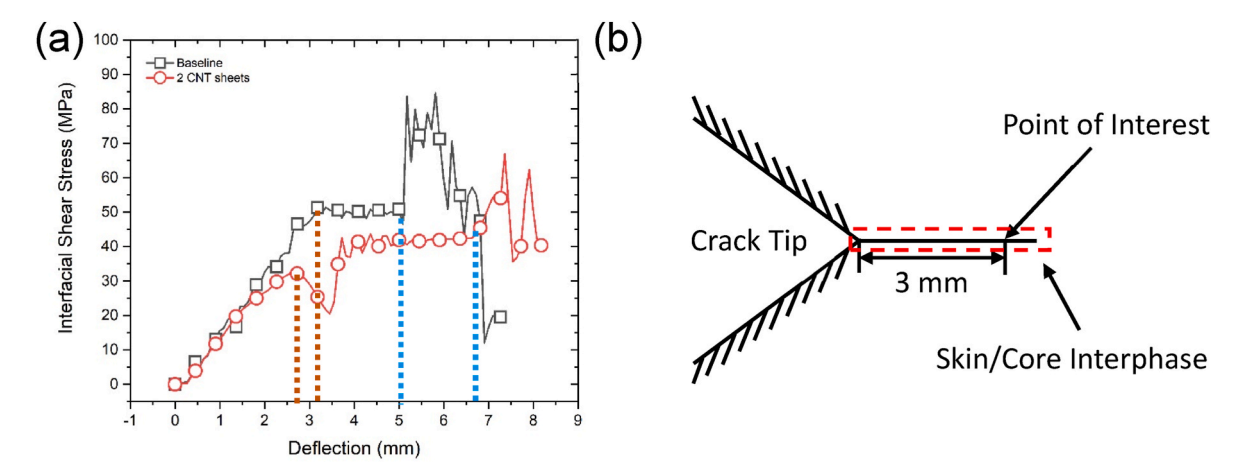


Fig. 9. IFSS versus deflection for the 2 MWNT sheets interleaved and baseline end-notched sandwich composites for an aspect ratio of 6:1: (a) IFSS at 3 mm in front of the crack tip, (b) schematic diagram of the crack tip in the skin/core interphase. Note: The brown dashed line indicates the 1st stage fracture initiation on the end-notch, and the blue dashed line indicates the 2nd stage fracture initiation on the crack tip. (For interpretation of the references to colour in this figure legend, the reader is referred to the Web version of this article.)

# 5. Discussion on the electrical and thermal conductance of the MWNT sheets interleaved sandwich composites and comparison with other MWNT/epoxy composites

Compared with other methods for enhancing the skin/core interphase of the sandwich composites, MWNT material is highly attractive for providing a high multi-functional performance [60]. For mechanical performance, a detailed summary of the MWNT sheets interleaved sandwich composites and a comparison with the commercial MWNT/epoxy composites are shown in Table 4. All the referenced work can represent typical cases of the MWNT modification on the skin/core interphase of sandwich composites and the MWNT sheets interleaved glass fiber composites.

In Table 4, there are two numerical values in row 2 column 13, and row 2 column 14 for enhancements of IFSS and energy absorption. These two IFSS enhancements (row 2 column 13) are the average values of the entire sandwich and the value near the stress concentration region of skin/core interphase at the 2nd stage fracture initiation (152.8 % and 244.2 %, respectively). The energy absorption enhancement (row 2 column 14) is the average value of the entire skin/core interphase and the entire sandwich composite specimen at the 2nd stage fracture initiation (132.6 % and 82.6 %, respectively).

We next compare our results with literature data. Chen et al. reported, a 94.6 % enhancement in the mode I fracture toughness of sandwich composite by electrostatic flocking 1 wt% MWNT on fabric surfaces. However, the testing speed of DCB is 20 mm/min, which is 40 times faster than our case, and a higher testing speed can positively affect the fracture initiation strength [65]. From the work of Patra et al., in which 0.3 wt% MWNT was dispersed in a resin matrix, and the MWNT/resin was infused into the raw materials, 34.6 % loading capacity and 55.0 % mode I fracture toughness enhancements were obtained. However, the aspect ratio for the debonding test is an essential factor for fracture initiation and propagation. Based on the Patra et al. investigation, a lower aspect ratio can increase IFSS on the skin/core interphase, thereby positively influencing the fracture mechanism.

Compared with the MWNT sheets interleaved sandwich composite and conventional-thin fiber-reinforced composite, interleaved MWNT sheets can enhance mode I fracture toughness on the fiber-reinforced composite plate and mode II fracture toughness on the sandwich composites. On the other hand, the functionally graded MWNT chemical-coated chopped carbon fiber mat cannot enhance the mechanical properties as much as interleaved MWNT sheets. However, this enhancing agent can significantly improve the electrical and thermal conductivity of the skin/core interphase. Furthermore, because a

sufficient volume fraction of carbon fiber on the skin/core interphase is acting as a base of the electric and thermal conductivity, MWNT can further enhance the conductivity.

An insight into the electrical and thermal conductivity of the laminated MWNT densified MWNT/polymer composite sheet coated on the PVC foam core surface of sandwich composites is discussed in this paragraph. The paper by Tan et al. showed that the densified MWNT sheets coated on PVC foam core achieved good thermal (~11  $W/(m \bullet K)$ ) and electrical conductivity (~8.3 × 10<sup>4</sup> S/m), with a high ultimate tensile strength of ~670 MPa [66]. The thickness of the densified MWNT sheets is approximately 200 nm [38]. Compared with the measured average thickness of the skin/core interphase ( $\sim$ 15  $\mu m$ ), the intention is to provide high electrical and thermal conductivity in the skin/core interphase region. Also, these estimations of electrical and thermal conductivities are based on the effective Young's modulus in the skin/core interphase of the CZM model (130 GPa). The true Young's modulus of the laminated densified MWNT sheets can be higher than these values. Also, Tan et al. give peak values for Young's modulus, ultimate tensile strength, thermal conductivity, and electrical conductivity of the laminated densified MWNT/polymer composite sheet that are 450 GPa, 7 TPa, 80  $W/(m \bullet K)$ , and  $9 \times 10^5$  S/m for a local fiber volume fraction of ~90 % [66]. Therefore, the actual mechanical electrical, and thermal properties of the laminated densified MWNT/polymer composite sheet should be similar. The electrical conductivity of the skin/core interphase region was measured as  $4.3 \times 10^4$  S/m. The actual value is on the same order of magnitudes as the lower limit of the estimated range (8.3  $\times$  10<sup>4</sup>–9  $\times$  10<sup>5</sup> S/m), based on the previous investigation [66-68]. The lower value than the theoretical estimated range is likely due to imperfections in the densified MWNT sheets. The measured electrical conductivity value, however, is still high, which is comparable to the higher values of electrical conductivity of conductive polymers used in composites  $(10-10^4 \text{ S/m})$  [69–71]. According to the investigation by Chu et al. [72], a meso/macroporous CNT paper developed for composite structures exhibits an electrical conductivity of  $7.8 \times 10^3$  S/m, capable of de-icing within 220 s at -22 °C. Zeng et al. [73] reported that a PVDF/CNTs/Ni composite film, suitable for engineering structures, demonstrates an EMI shielding property of 102.8 dB mm<sup>-1</sup>, with electrical conductivity ranging from 1.1 to  $2.3 \times 10^2$  S/m. Furthermore, Wang et al. [74] showed that dispersing CNTs in epoxy at concentrations of 0.2-1.8 wt% results in an electrical conductivity range of 10<sup>-3</sup> to 10<sup>-5</sup> S/m, applicable for structural health monitoring. These results indicate that laminated MWNT sheets interleaved within sandwich composites provide both electrical and thermal conductivities higher than those of conductive polymers. This enhancement paves the

Reference	Composite Material	Interphase Material	Process method	wt%	TY/AR/TS	$\Delta \sigma_f/\sigma_{fc}$	$\Delta G_{II}/G_{IIc}$	$\Delta G_I/G_{Ic}$	$\Delta k_H/k_{Hc}$	$\Delta K_{II}/K_{IIc}$	$\Delta K_I/K_{Ic}$	$TY/AR/TS \qquad \Delta \sigma_f/\sigma_{fc} \qquad \Delta G_{II}/G_{ILc} \qquad \Delta G_{II}/G_{Ic} \qquad \Delta K_{II}/K_{IIc} \qquad \Delta K_{II}/K_{ILc} \qquad \Delta K_{II}/K_{fc} \qquad \Delta T_{IISSc}$	$\Delta G_{se}/G_{sec}$
This work	GF/PVC-SC	MWNT sheets	Interleaved	$\sim \! 0.084$	ENF/6:1/0.5	36.8	125.7	127.3	50.0	110.3	86.0	Entire sandwich: 244.2/	Entire interphase: 132.6/
					mm/min							Stress concentration: 152.8	Entire sandwich: 82.6
Chen et al.	CF/H-SC	MWNT forest	Electrostatic	1.5	DCB/-/20	1	1	94.6	1	1	1	1	1
[61]			flocking		mm/min								
Chen et al.	GF/PVC-SC	MWNT-C/	Chemical &	1.5	DCB/-/2	19.1	I	44.9	ı	1	1	I	I
[62]		CCFM	interleaved		mm/min								
Patra et al.	GF/PVC-SC	MWNT	Dispersion	1.5	DCB/ - /0.5	1	ı	1	1	1	34.3	1	1
[32]		/epoxy			mm/min								
Patra et al.	GF/PVC-SC	MWNT	Dispersion	0.3	MMB/4:1/0.5	>34.6	I	1	ı	$K_{mix} > 55.0$	0	I	I
[63]		/epoxy			mm/min								
Cheng et al.	GP	MWNT/epoxy	Interleaved	1	ENF/5:1/1	28.5	I	1	1	28.46	126.2	34.0	ı
[64]		sheets			mm/min								
					DCB/=/1 mm/min								
Koirala et al.	CFRC	MWNT sheets	Interleaved	0.048	DCB/ - /1	ı	1	ı	1	1	57.0	30	1
[38]					mm/min								

of: flexural strength,  $G_I$ : mode II fracture toughness,  $k_I$ : stress intensity factor,  $K_{II}$ : fracture toughness at 2nd fracture initiation stage,  $\tau_{IISS}$ : interfacial shear stress,  $G_{ac}$ : energy absorption (Unit for mechanical properties is Note: 1. wt%: weight fraction of the MWNT, AR: aspect ratio of the experimental testing, TY: testing type, TS: testing speed, ENF: end-notched flexural test, DCB: double cantilever beam test, MMB: mix mode bending test, CFRC: carbon fiber reinforced composite, SC: sandwich composite, GP: GFRC prepreg, GF/PVC; GFRC skin/PVC foam core, CF/H: GFRC skin/honeycomb foam core, MWNT-C/CCFM: MWNT-COOH/chopped glass fiber mat the percentage (%)); 2.

way for exploring applications such as lightning protection, structural health monitoring, and de-icing in strong, lightweight sandwich composite structures across various fields, including aerospace and wind energy.

The primary challenge in this research is achieving consistent densification of MWNT sheets into a Xerogel layer on PVC foam, especially for large sandwich panels. Developing a proper densification process is crucial to enhance uniformity and efficiency across larger panels, thereby fulfilling the requirements for scaled-up production in the composites industry.

# 6. Conclusion

In this work, we prepared end-notched sandwich composites by VARTM process, then measured the mode I and mode II fracture criteria by ENF tests, following analysis of mechanical properties of the crack tip and skin/core interphase by CZM. To strengthen the fracture toughness and IFSS, ultra-thin MWNT sheets (1-4 plys) from an MWNT forest were interleaved and then densified in the skin/core interphase region of the sandwich composites. After the resin was impregnated in the composite laminates and cured in an autoclave, the continuous and highly dense MWNT sheets were connected to PVC foam and glass fabric surfaces by crosslinking with polymer chains. Two MWNT sheets (~0.084 wt%) interleaved sandwich composites possess the best performance (36.8 % increase in flexural strength; 127.3 % and 125.7 % increases in mode I & II fracture toughness values, respectively; and 152.8 % increase in IFSS) among all types of sandwich composites. When interleaving more than two layers of MWNT sheets (>0.084 wt%) in the skin/core interphase region, shearing between MWNT sheets can lead to early fracture initiation, hence reducing the mechanical properties of the sandwich composite. The advantages of the interleaving process for laminated MWNT sheets are cost-effectiveness, easy scalability, and reduction in composite weight, along with better mechanical performance than for materials produced by MWNT dispersion processes.

The CZM fracture model uses a cohesive solid element layer on the notched and unnotched skin/core interphase to achieve more realistic conditions, considering the skin/core jam for the end-notched region. The FEM model reveals the local mechanical behavior of the skin, core, crack tip, and skin/core interphase. Interleaving the MWNT sheets on the skin/core interphase can reduce the stress level on the skin and core, hence delaying fracture initiation and propagation for the core. Also, a lower IFSS on the crack tip and a sufficiently high IFSS on the skin/core interphase under the loading pin is captured. This indicates that the MWNT sheets can delay fracture initiation on the crack tip and enhance the load capacity of the entire sandwich structure. In addition, a sinusoidal form of IFSS is captured for the skin/core interphase, and the MWNT sheets can provide significantly enhanced stability concerning crack propagation.

MWNT also enhanced the electrical conductivity of the cured resin in the skin/core interphase region. The measured electrical conductivity of the skin/core interphase region is  $4.3 \times 10^4$  S/m, which is on the same order of magnitude as the electrical conductivity  $(10-10^4$  S/m) of a highly conductive polymer [69–71]. Replacing conventional conductive materials with MWNT-filled polymers reported herein can increase flexibility and reduce the structure's weight. Furthermore, the densified MWNT layer in the skin/core interface provides additional functions, such as EMI shielding, de-icing, and structural health monitoring.

Herein, the MWNT sheets interleaved sandwich composite has been shown to have significantly increased the IFSS (an increase of 152.8 % over the baseline); it is suitable for structural applications that require high interfacial strength at the interface. The insertion of MWNT sheets also effectively prevents or delays the damage formation at the core/skin interface in sandwich composites. Furthermore, the laminated MWNT sheets process is easily scalable and cost-effective, paving the way for such diverse applications as aerospace, wind energy, sports gear, and ships.

# CRediT authorship contribution statement

Dongyang Cao: Writing – original draft, Methodology, Investigation, Formal analysis, Data curation, Conceptualization. Tingge Xu: Formal analysis, Conceptualization. Mengmeng Zhang: Investigation, Data curation. Zhong Wang: Investigation, Data curation. D. Todd Griffith: Writing – review & editing, Visualization, Validation, Funding acquisition. Samit Roy: Writing – review & editing, Visualization, Validation, Funding acquisition. Ray H. Baughman: Writing – review & editing, Validation, Funding acquisition. Hongbing Lu: Writing – review & editing, Visualization, Validation, Supervision, Project administration, Methodology, Funding acquisition, Conceptualization.

# Declaration of competing interest

The authors declare that they have no known competing financial interests or personal relationships that could have appeared to influence the work reported in this paper.

### Data availability

Data will be made available on request.

# Acknowledgment

We acknowledge the support of NSF under 2219347 & 1636306, the NSF WindStar I/UCRC Center (under NSF IIP-1362033 and IIP-1916776), the Department of Energy under DE-NA0003962 & DE-NA-0003525, Air Force under FA8650-23-C-5006, Naval ONR/STTR N68335-18-C-0368, Air Force Office of Scientific Research under N68335–19C-0303 & FA9550-21-1-0455, Robert A. Welch Foundation grant no. AT-0029, and the Louis A. Beecherl Jr. chair. We thank Lintec America, DIAB, Westlake Epoxy, and TPI Composites for supplying the MWNT forest, foam core, resin, and glass fiber, respectively, used to prepare the sandwich composites.

# Appendix A. Supplementary data

Supplementary data to this article can be found online at https://doi.org/10.1016/j.compositesb.2024.111496.

# References

- [1] Bensattalah T, Bouakkaz K, Zidour M, Daouadji TH. Critical buckling loads of carbon nanotube embedded in Kerr's medium. Adv Nano Res 2018;6(4):339–56. https://doi.org/10.12989/ANR.2018.6.4.339.
- [2] Belkacem A, Tahar HD, Abderrezak R, et al. Mechanical buckling analysis of hybrid laminated composite plates under different boundary conditions. Struct Eng Mech 2018;66(6):761. https://doi.org/10.12989/SEM.2018.66.6.761.
- [3] Ghorbanpour-Arani AA, Khoddami Maraghi Z, Ghorbanpour Arani A. The frequency response of intelligent composite sandwich plate under biaxial in-plane forces. J Solid Mech 2023;15(1):1–18. https://doi.org/10.22034/ JSM.2020.1895607.1563.
- [4] Bouazza M, Amara K, Zidour M, Abedlouahed T, Bedia A, Abbas E. Thermal effect on buckling of multiwalled carbon nanotubes using different gradient elasticity theories. Nanosci Nanotechnol 2014;4(2):27–33. https://doi.org/10.5923/j. nn.20140402.02.
- [5] Birman V, Kardomateas GA. Review of current trends in research and applications of sandwich structures. Compos B Eng 2018;142:221–40. https://doi.org/10.1016/ J.COMPOSITESB.2018.01.027.
- [6] Cao D, Malakooti S, Kulkarni VN, Ren Y, Lu H. Nanoindentation measurement of core-skin interphase viscoelastic properties in a sandwich glass composite. Mech Time-Dependent Mater 2020. https://doi.org/10.1007/s11043-020-09448-y. Published online.
- [7] Cao Dongyang, Malakooti Sadeq, Kulkarni Vijay N, Ren Yao, Liu Yingjian, Nie Xu, Qian Dong, Todd D, Griffith HL. The effect of resin uptake on the flexural properties of compression molded sandwich composites. Wind Energy 2021:4–11. Published online.
- [8] Chai GB, Zhu S. A review of low-velocity impact on sandwich structures. Proc Inst Mech Eng Part L 2011;225(4):207–30. https://doi.org/10.1177/ 1464420711409985.

- [9] Mallikarjuna Kant T. A critical review and some results of recently developed refined theories of fiber-reinforced laminated composites and sandwiches. Compos Struct 1993;23(4):293–312. https://doi.org/10.1016/0263-8223(93)90230-N.
- [10] Bozkurt ÖY, Bulut M, Erkliğ A, Faydh WA. Axial and lateral buckling analysis of fiber reinforced S-glass/epoxy composites containing nano-clay particles. Compos B Eng 2019;158:82–91. https://doi.org/10.1016/J.COMPOSITESB.2018.09.043.
- [11] Nanayakkara AM, Feih S, Mouritz AP. Improving the fracture resistance of sandwich composite T-joints by z-pinning. Compos Struct 2013;96:207–15. https://doi.org/10.1016/J.COMPSTRUCT.2012.09.029.
- [12] Mitra N. A methodology for improving shear performance of marine grade sandwich composites: sandwich composite panel with shear key. Compos Struct 2010;92(5):1065–72. https://doi.org/10.1016/J.COMPSTRUCT.2009.10.005.
- [13] Yalkin HE, Icten BM, Alpyildiz T. Enhanced mechanical performance of foam core sandwich composites with through the thickness reinforced core. Compos B Eng 2015;79:383–91. https://doi.org/10.1016/J.COMPOSITESB.2015.04.055.
- [14] Yao J, Zhang T, Niu Y. Effect of curing time on phase morphology and fracture toughness of PEK-C film interleaved carbon fibre/epoxy composite laminates. Compos Struct 2020;248:112550. https://doi.org/10.1016/J. COMPSTRUCT.2020.112550.
- [15] Chen Q, Linghu T, Gao Y, et al. Mechanical properties in glass fiber PVC-foam sandwich structures from different chopped fiber interfacial reinforcement through vacuum-assisted resin transfer molding (VARTM) processing. Compos Sci Technol 2017;144:202–7. https://doi.org/10.1016/J.COMPSCITECH.2017.03.033.
- [16] Haghparast E, Ghorbanpour-Arani A, Arani AG. 101142/S1758825120500787. Effect of fluid-structure interaction on vibration of moving sandwich plate with balsa wood core and nanocomposite face sheets, vol. 12; 2020. https://doi.org/ 10.1142/S1758825120500787. 7.
- [17] Hou S, Li T, Jia Z, Wang L. Mechanical properties of sandwich composites with 3d-printed auxetic and non-auxetic lattice cores under low velocity impact. Mater Des 2018;160:1305–21. https://doi.org/10.1016/J.MATDES.2018.11.002.
- [18] Nanayakkara A, Feih S, Mouritz AP. Experimental analysis of the through-thickness compression properties of z-pinned sandwich composites. Compos Part A Appl Sci Manuf 2011;42(11):1673–80. https://doi.org/10.1016/j. compositesa.2011.07.020.
- [19] Juliyana M, Santhana Krishnan R. Development of button shear keys to improve the debonding resistance of sandwich composite panel. Mater Today Proc 2019;16 (2):720-7. www.sciencedirect.com.
- [20] Majumdar P, Srinivasagupta D, Mahfuz H, Joseph B, Thomas MM, Christensen S. Effect of processing conditions and material properties on the debond fracture toughness of foam-core sandwich composites: experimental optimization. Compos Part A Appl Sci Manuf 2003;34(11):1097–104. https://doi.org/10.1016/S1359-835X(03)00207-0.
- [21] Narayana J, Gupta Burela R. A review of recent research on multifunctional composite materials and structures with their applications, vol. 5; 2018. www.s jencedirect.comwww.materialstoday.com/proceedings.
- [22] Ghorbanpour-Arani AH, Rastgoo A, Sharafi MM, Kolahchi R, Ghorbanpour Arani A. Nonlocal viscoelasticity based vibration of double viscoelastic piezoelectric nanobeam systems. Meccanica 2016;51(1):25–40. https://doi.org/10.1007/ S11012-014-9991-0/FIGURES/8.
- [23] Ghorbanpour-Arani AH, Rastgoo A, Hafizi Bidgoli A, Kolahchi R, Ghorbanpour Arani A. Wave propagation of coupled double-DWBNNTs conveying fluid-systems using different nonlocal surface piezoelasticity theories. Mech Adv Mater Struct 2017;24(14):1159–79. https://doi.org/10.1080/15376494.2016.1227488.
- [24] Ghorbanpour-Arani AH, Abdollahian M, Ghorbanpour Arani A. Nonlinear dynamic analysis of temperature-dependent functionally graded magnetostrictive sandwich nanobeams using different beam theories. J Braz Soc Mech Sci Eng 2020;42(6): 1–20. https://doi.org/10.1007/S40430-020-02400-8/METRICS.
- [25] Ghorbanpour Arani A, Jamali M, Ghorbanpour-Arani AH, Kolahchi R, Mosayyebi M. Electro-magneto wave propagation analysis of viscoelastic sandwich nanoplates considering surface effects. Proc Inst Mech Eng C J Mech Eng Sci. 2017; 231(2):387–403. https://doi.org/10.1177/0954406215627830/ASSET/IMAGES/ LARGE/10.1177\_0954406215627830-FIG9.JPEG.
- [26] Wang X, Xu T, Andrade MJ De, et al. The interfacial shear strength of carbon nanotube sheet modified carbon fiber composites. In: Challenges in mechanics of time-dependent materials. Vol 2. Conference proceedings of the society for experimental mechanics series; 2021. https://doi.org/10.1007/978-3-030-59542-5.4
- [27] Peigney A, Laurent C, Flahaut E, Bacsa RR, Rousset A. Specific surface area of carbon nanotubes and bundles of carbon nanotubes. Carbon N Y 2001;39(4): 507–14. https://doi.org/10.1016/S0008-6223(00)00155-X.
- [28] Treacy MMJ, Ebbesen TW, Gibson JM. Exceptionally high Young's modulus observed for individual carbon nanotubes. Nature 1996;381(6584):678–80. https://doi.org/10.1038/381678a0.
- [29] Demczyk BG, Wang YM, Cumings J, et al. Direct mechanical measurement of the tensile strength and elastic modulus of multiwalled carbon nanotubes. Mater Sci Eng 2002;334(1–2):173–8. https://doi.org/10.1016/S0921-5093(01)01807-X.
- [30] Arani AG, Haghparast E, Ghorbanpour Arani AH. Size-dependent vibration of double-bonded carbon nanotube-reinforced composite microtubes conveying fluid under longitudinal magnetic field. Polym Compos 2016;37(5):1375–83. https:// doi.org/10.1002/PC.23306.
- [31] D MM, Gallman J, Johnson V, Garcia E, Tai J, Young R. N+3 small commercial efficient and quiet transportation for year 2030-2035. http://www.sti.nasa.gov; 2010.
- [32] Jakubinek MB, Ashrafi B, Zhang Y, et al. Single-walled carbon nanotube-epoxy composites for structural and conductive aerospace adhesives. Compos B Eng 2015; 69:87–93. https://doi.org/10.1016/j.compositesb.2014.09.022.

- [33] Rose Abraham A, George SC, Haghi AK. Carbon nanotubes: functionalization and potential applications..
- [34] Harussani MM, Sapuan SM, Nadeem G, Rafin T, Kirubaanand W. Recent applications of carbon-based composites in defence industry: a review. Defence Technology 2022;18(8):1281–300. https://doi.org/10.1016/j.dt.2022.03.006.
- [35] Patra A, Mitra N. Interface fracture of sandwich composites: influence of MWCNT sonicated epoxy resin. Compos Sci Technol 2014;101:94–101. https://doi.org/ 10.1016/J.COMPSCITECH.2014.07.006.
- [36] Sánchez M, Campo M, Jiménez-Suárez A, Ureña A. Effect of the carbon nanotube functionalization on flexural properties of multiscale carbon fiber/epoxy composites manufactured by VARIM. Compos B Eng 2013;45(1):1613–9. https:// doi.org/10.1016/J.COMPOSITESB.2012.09.063.
- [37] Han X, Zhao Y, Sun JM, Li Y, Zhang JD, Hao Y. Effect of graphene oxide addition on the interlaminar shear property of carbon fiber-reinforced epoxy composites. N Carbon Mater 2017;32(1):48–55. https://doi.org/10.1016/S1872-5805(17) 60107-0
- [38] Koirala P, van de Werken N, Lu H, Baughman RH, Ovalle-Robles R, Tehrani M. Using ultra-thin interlaminar carbon nanotube sheets to enhance the mechanical and electrical properties of carbon fiber reinforced polymer composites. Compos B Eng 2021;216. https://doi.org/10.1016/j.compositesb.2021.108842.
- [39] Zheng N, Huang Y, Liu HY, Gao J, Mai YW. Improvement of interlaminar fracture toughness in carbon fiber/epoxy composites with carbon nanotubes/polysulfone interleaves. Compos Sci Technol 2017;140:8–15. https://doi.org/10.1016/j. compscitech 2016.12.017
- [40] Li Z, Wang Z, Lu W, Zhou X, Suo T. Loading rate dependence of mode II fracture toughness in laminated composites reinforced by carbon nanotube films. Compos Sci Technol 2021;215. https://doi.org/10.1016/j.compscitech.2021.109005.
- [41] Kim SH, Haines CS, Li N, et al. Harvesting electrical energy from carbon nanotube yarn twist. Sci (1979) 2017;357(6353):773–8. https://doi.org/10.1126/SCIENCE. AAM8771/SUPPL\_FILE/AAM8771S2.MP4.
- [42] ASTM International. Standard test method for determination of the mode II interlaminar fracture toughness of unidirectional fiber-reinforced polymer matrix composites 1, 2019. https://doi.org/10.1520/D7905 D7905M-19.
- [43] Peters WH, Ranson WF. Digital imaging techniques in experimental stress analysis. Opt Eng 1982;21(3). https://doi.org/10.1117/12.7972925.
- [44] Sutton M, Wolters W, Peters W, Ranson W, McNeill S. Determination of displacements using an improved digital correlation method. Image Vis Comput 1983;1(3):133–9. https://doi.org/10.1016/0262-8856(83)90064-1.
- [45] Vend Roux G, Knauss WG. Submicron deformation field measurements: Part 2. Improved digital image correlation. Exp Mech 1998;38(2):86–92. https://doi.org/10.1007/BF02321649.
- [46] Lu H, Cary PD. Deformation measurements by digital image correlation: implementation of a second-order displacement gradient. Exp Mech 2000;40(4): 393–400. https://doi.org/10.1007/BF02326485.
- [47] Arruda MRT, Trombini M, Pagani A. Implicit to explicit algorithm for ABAQUS standard user-subroutine UMAT for a 3D hashin-based orthotropic damage model. Appl Sci 2023;13(2). https://doi.org/10.3390/app13021155.
- [48] Xu T. Characterization and modeling of mechanical behavior of polymers and composites at small scales by nanoindentation. 2017.
- [49] Ravindranath PK, Roy S, Unnikrishnan V, et al. A multiscale model to study the enhancement in the compressive strength of multi-walled CNT sheet overwrapped carbon fiber composites. Compos Struct 2019;219(July):170–8. https://doi.org/ 10.1016/j.compstruct.2019.03.065
- [50] Fisher FT, Bradshaw RD, Brinson LC. Fiber waviness in nanotube-reinforced polymer composites—I: modulus predictions using effective nanotube properties. Compos Sci Technol 2003;63(11):1689–703. https://doi.org/10.1016/S0266-3538 (33)00069-1
- [51] Wan Jialai, Qiao Pizhong. Fracture analysis of shear deformable Bi-material interface. J Eng Mech 2006;132(3):306–16. https://web-p-ebscohost-com.libpro xy.utdallas.edu/ehost/pdfviewer/pdfviewer?vid=0&sid=c1efe4cf-59e3-42e5-9 c9d-b7af1e73ed3f%40redis. [Accessed 12 May 2022].
- [52] Gafour YAAMT. Porosity-dependent free vibration analysis of FG nanobeam using non-local shear deformation and energy principle. Adv Nano Res 2020;8(1):37–47. https://doi.org/10.12989/ANR.2020.8.1.037.
- [53] Benahmed A, Fahsi B, Benzair A, et al. Critical buckling of functionally graded nanoscale beam with porosities using nonlocal higher-order shear deformation. Struct Eng Mech 2019;69(4):457. https://doi.org/10.12989/SEM.2019.69.4.457.
- [54] Zerrouki R, Karas A, Zidour M, et al. Effect of nonlinear FG-CNT distribution on mechanical properties of functionally graded nano-composite beam. Struct Eng Mech 2021;78(2):117. https://doi.org/10.12989/SEM.2021.78.2.117.

- [55] Chemi A, Heireche H, Zidour M, Rakrak K, Bousahla AA. Critical buckling load of chiral double-walled carbon nanotube using non-local theory elasticity. Adv Nano Res 2015;3(4):193–206. https://doi.org/10.12989/ANR.2015.3.4.193.
- [56] Chyanbin H, Hu JS. Stress intensity factors and energy release rates of delaminations in composite laminates. Eng Fract Mech 1992;42(6):977–88. https://doi.org/10.1016/0013-7944(92)90137-4.
- [57] Bensattalah T, Zidour M, Daouadji TH, et al. Theoretical analysis of chirality and scale effects on critical buckling load of zigzag triple walled carbon nanotubes under axial compression embedded in polymeric matrix. Struct Eng Mech 2019;70 (3):269. https://doi.org/10.12989/SEM.2019.70.3.269.
- [58] Bensattalah T, Hamidi A, Bouakkaz K, Zidour M, Daouadji TH. Critical buckling load of triple-walled carbon nanotube based on nonlocal elasticity theory. J Nano Res 2020;62:108–19. https://doi.org/10.4028/WWW.SCIENTIFIC.NET/ JNANOR.62.108.
- [59] Crisafulli A, Khodayari A, Mohammadnejad S, Fasano M. Sliding dynamics of parallel graphene sheets: effect of geometry and van der Waals interactions on nano-spring behavior. Crystals 2018;8(4):149. https://doi.org/10.3390/ CRYSTRA00140
- [60] Soni SK, Thomas B, Kar VR. A comprehensive review on CNTs and CNT-reinforced composites: syntheses, characteristics and applications. Mater Today Commun 2020;25. https://doi.org/10.1016/J.MTCOMM.2020.101546.
- [61] Chen C, Li Y, Gu Y, Li M, Zhang Z. Effect of MWCNTs added by electrostatic flocking method on adhesion of carbon fiber prepreg/Nomex honeycomb sandwich composites. Mater Des 2017;127:15–21. https://doi.org/10.1016/J. MATDES 2017.04.025
- [62] Chen Q, Du S, Jiang Z, Liu Y, Du R, Zhao G. Mechanical properties of foam sandwich with chopped-glass-fiber/carbon nanotube reinforced hierarchical structure interlayer. Polym Compos 2020;41(8):3411–20. https://doi.org/ 10.1002/PC 25630
- [63] Patra AK, Mitra N. Mixed-mode fracture of sandwich composites: performance improvement with multiwalled carbon nanotube sonicated resin. J Sandw Struct Mater 2018;20(3):379–95. https://doi.org/10.1177/1099636216656485/ASSET/ IMAGES/LARGE/10.1177 1099636216656485-FIG2\_JPEG.
- [64] Han CL, Wang GD, Li N, Wang M, Liu XL, Ma JH. Study on interlaminar performance of CNTs/epoxy film enhanced GFRP under low-temperature cycle. Compos Struct 2021;272:114191. https://doi.org/10.1016/J. COMPSTRUCT.2021.114191.
- [65] Scudamore RJ, Cantwell WJ. The effect of moisture and loading rate on the interfacial fracture properties of sandwich structures. Polym Compos 2002;23(3): 406–17. https://doi.org/10.1002/PC.10442.
- [66] Tan W, Stallard JC, Smail FR, Boies AM, Fleck NA. The mechanical and electrical properties of direct-spun carbon nanotube mat-epoxy composites. Carbon N Y 2019;150:489–504. https://doi.org/10.1016/J.CARBON.2019.04.118.
- [67] Yadav A, Godara RK, Bhardwaj G, Patil RU, Singh SK, Khanna K. A review on fracture analysis of CNT/graphene reinforced composites for structural applications. Arch Comput Methods Eng 2022;29(1):545–82. https://doi.org/ 10.1007/s11831-021-09650-2.
- [68] Islam MH, Afroj S, Uddin MA, Andreeva DV, Novoselov KS, Karim N. Graphene and CNT-based smart fiber-reinforced composites: a review. Adv Funct Mater 2022;32 (40), https://doi.org/10.1002/adfm.202205723.
- [69] Wang M, Tang XH, Cai JH, Wu H, Shen J Bin, Guo SY. Construction, mechanism and prospective of conductive polymer composites with multiple interfaces for electromagnetic interference shielding: a review. Carbon N Y 2021;177:377–402. https://doi.org/10.1016/J.CARBON.2021.02.047.
- [70] Xu S, Shi XL, Dargusch M, Di C, Zou J, Chen ZG. Conducting polymer-based flexible thermoelectric materials and devices: from mechanisms to applications. Prog Mater Sci 2021;121:100840. https://doi.org/10.1016/J.PMATSCI.2021.100840.
- [71] Odey Magu T, Louis H, Magu TO. A review on conducting polymers-based composites for energy storage application A review on conducting polymers-based composites for energy storage ApplicationT. J Chem Rev 2019;(1):19–34. https://doi.org/10.33945/SAMI/JCR.2019.1.1934.
- [72] Chu H, Zhang Z, Liu Y, Leng J. Self-heating fiber reinforced polymer composite using meso/macropore carbon nanotube paper and its application in deicing. Carbon N Y 2014;66:154–63. https://doi.org/10.1016/J.CARBON.2013.08.053.
- [73] Zeng S, Li X, Li M, et al. Flexible PVDF/CNTs/Ni@CNTs composite films possessing excellent electromagnetic interference shielding and mechanical properties under heat treatment. Carbon N Y 2019;155:34–43. https://doi.org/10.1016/J. CARBON.2019.08.024.
- [74] Wang Y, Wang Y, Wan B, Han B, Cai G, Li Z. Properties and mechanisms of self-sensing carbon nanofibers/epoxy composites for structural health monitoring. Compos Struct 2018;200:669–78. https://doi.org/10.1016/J. COMPSTRUCT 2018 05 151